ADVANCED ELECTRONIC MATERIALS
www.advelectronicmat.de

Flexible, Transparent, Sensitive, and Crosstalk-Free Capacitive Tactile Sensor Array Based on Graphene Electrodes and Air Dielectric

Soonjae Pyo, Jungwook Choi, and Jongbaeg Kim**

The development of sensitive, flexible, and transparent tactile sensors is of great interest for next-generation flexible displays and human–machine interfaces. Although a few materials and structural designs have been previously developed for high-performance tactile sensors, achieving flexibility, full transparency, and highly sensitive multipoint recognition without crosstalk remains a significant challenge for such systems. This work demonstrates a capacitive tactile sensor composed of two sets of facing graphene electrodes separated by spacers, which forms an air dielectric between them. The air gap facilitates more effective deformation of the top graphene electrode under pressure compared to typical elastomer dielectrics, resulting in a high sensitivity of 6.55% kPa^{-1} and a fast response time of ≈70 ms. Taking advantage of the remarkable properties of graphene for electrode usage, the tactile sensor presents sufficient transparency (over 70% at 550 nm) as well as excellent electrical and mechanical flexibility for 500 cycles at a bending radius of 8 mm. Simulated and experimental results validate that the isolation of each tactile cell by the spacers allows the pixelated sensor array to recognize the spatial distribution of applied pressure without crosstalk. The proposed sensor would be a promising candidate for tactile sensing components that require both flexibility and transparency.

1. Introduction

In recent years, flexible, stretchable, or transparent devices have received significant attention as various next-generation electronic systems, such as transistors,[1] sensors,[2] and supercapacitors.[3] Among these potential applications, tactile sensors, which can quantify information in response to physical contact between a sensor and some object, have been actively explored for diverse purposes ranging from flexible touch screens[4,5] to electronic skin.[6,7] High sensitivity, multipoint recognition, optical transparency, and mechanical flexibility of the sensor are considered as essential requirements for use in future tactile sensing applications. To fulfill these demands, a broad range of materials, fabrication processes, and structural designs of the tactile sensor have been developed,[8] while sensing principles are mainly classified as either resistive[9–11] or capacitive types.[12–14] Many of resistive sensors use nanomaterial-embedded composites and exploit changes in contact resistance between the nanomaterials in the composite matrix (such as elastomer) under pressure loading, showing improved pressure sensitivity and mechanical flexibility compared to silicon- or metal-based piezoresistive sensors.[15] However, resistive tactile sensors suffer from signal drift due to temperature changes and require high power consumption. In addition, complicated circuit arrangement for multipoint recognition is regarded as a drawback to be addressed.[7,16]

Compared to resistive tactile sensing mechanisms, capacitive tactile sensors have advantages in terms of temperature independence, low power consumption, stability against long-term signal drift, and easy multipoint recognition by simple assembly of row and column electrodes.[16,17] In general, the structure of a capacitive sensor consists of two parallel electrodes with a dielectric layer between them. Highly compressible dielectric materials are essential to achieve high sensitivity; a lower Young's modulus of the dielectric leads to greater deformation when pressure is applied to the sensor, resulting in a larger change in capacitance. Accordingly, considerable efforts have been devoted to using elastomers with low Young's modulus as dielectric materials, including polydimethylsiloxane (PDMS),[18] polyurethane,[19] or Ecoflex.[12] However, these low-modulus elastomers also tend to have high viscoelasticity, slowing their response and relaxation times.[20] To overcome this limitation and further improve the sensitivity, a few tactile sensors make use of the strategy of structuring the dielectric layer by fabricating a microstructured surface in an orderly fashion.[7,20,21] The microstructured dielectric layer led to much higher sensitivity and faster response/relaxation time by allowing a larger deformation compared to conventional capacitive sensors with a plain dielectric layer under equal applied pressure. Nevertheless,

Dr. S. Pyo, Prof. J. Kim
School of Mechanical Engineering
Yonsei University
50 Yonsei-ro, Seodaemun-gu, Seoul 03722, Republic of Korea
E-mail: kimjb@yonsei.ac.kr
Prof. J. Choi
School of Mechanical Engineering
Yeungnam University
280 Daehak-ro, Gyeongsan, Gyeongbuk 38541, Republic of Korea
E-mail: jwc@yu.ac.kr

DOI: 10.1002/aelm.201700427

such dielectric design has inherent drawbacks, such as complicated fabrication, crosstalk between adjacent cells, and deterioration of transparency.[20,21] These drawbacks can be improved by replacing the dielectric layer with an air gap between the surrounding spacers in each tactile cell. The air gap would enable the top electrode to be effectively deformed under pressure, unlike elastomer dielectrics with energy dissipation by material damping. In parallel, the spacers, which surround each tactile cell with a higher rigidity than the other structures, limit the deformation of neighboring top electrodes that are not subjected to pressure application. Therefore, structural design, such as the air gap and spacer, would offer high sensitivity, hysteresis- and crosstalk-free recognition of external pressure with rapid response/relaxation time, and minimal loss of flexibility and transparency of the sensor.

Another limiting factor of existing capacitive sensors is that most of them still rely on opaque or brittle materials as electrodes, thereby impeding their application toward truly flexible and transparent tactile sensors. The substrate and electrodes regulate the flexibility and transparency of the entire capacitive tactile sensor, highlighting the importance of careful electrode material selection. Of the various candidates for electrodes in tactile sensors, monolayer graphene is a promising material when flexibility and transparency are required. Given its high fracture strain (>20%), low sheet resistance (≈300 Ω sq^{-1}), and high transmittance (≈97.5%),[22] many graphene-based tactile sensors have been reported thus far, but most of these utilized graphene as a piezoresistive or resistive sensing element.[23–25] Although previous works have shown high performance with sufficient flexibility and transparency, these devices still have the limitations of conventional piezoresistive and resistive tactile sensors. Thus, the development of a tactile sensor that not only overcomes the limitations of existing devices but also provides improved performance is highly desired.

Here, we present a capacitive tactile sensor comprised of monolayer graphene electrodes that are separated by spacers which form air gaps. The graphene electrodes are patterned and assembled on polyethylene terephthalate (PET) substrate, while PDMS and SU-8 serve as the dielectric and spacer between facing graphene electrodes, respectively. Based on the outstanding properties of graphene and the structural design of the air gap, the tactile sensor exhibits mechanical flexibility and optical transparency in the visible range, along with high pressure sensitivity (6.55% kPa^{-1}), rapid response (≈70 ms), and high stability over 2500 cycles of loading/unloading. We also demonstrated a pixelated sensor array for pressure mapping without any significant crosstalk between adjacent cells. At the same time, our tactile sensor shows resistance to other external stimuli such as changes in temperature and external bending without significant signal drift, and high reliability against repeated deformation of 500 cycles at a bending radius of 8 mm is demonstrated.

2. Results and Discussion

Figure 1a shows a schematic of the flexible, transparent capacitive tactile sensor, consisting of two graphene-patterned PET layers, PDMS insulator, and SU-8 spacers (see Experimental Section and Figure S1, Supporting Information for the fabrication process). The patterned graphene electrodes on the top and bottom PET films are placed orthogonal to each other, so that each crossing area between facing graphene layers forms a tactile cell in an array. The top and cross-sectional views of a single cell and its dimensions are depicted in Figure 1b. Two graphene electrodes on the 175 μm thick top and bottom PET films constitute a sensing capacitive cell, separated by a dielectric layer of 20 μm (10 μm thick PDMS layer and 10 μm thick air gap). The sizes of a single cell and the overlapped area between facing graphene electrodes are $4500 \times 4500\ \mu m^2$ and $1500 \times 1500\ \mu m^2$, respectively. When pressure is applied to the top PET film, the gap between the top and bottom layer decreases. As a result, the capacitance between the two graphene electrodes increases, enabling the magnitude of input pressure to be measured through changes in the capacitance. Furthermore, each tactile cell accurately recognizes the pressure regardless of the force applied on adjacent cells, because the four surrounding SU-8 spacers minimize crosstalk. The image in Figure 1c shows the fabricated tactile sensor, which is entirely transparent across all parts of the PET film. Figure 1d,e shows enlarged optical microscope and scanning electron microscope (SEM) images of the sensor, clearly denoting the patterned graphene and spacer.

To confirm successful transfer and patterning of graphene, we collected Raman spectra of graphene positioned on both SiO_2 and PET substrates with 532 nm laser excitation. A Raman spectrum of the monolayer graphene on SiO_2 shows two distinctive peaks, a G-band at ≈1584 cm^{-1} and a 2D-band at ≈2680 cm^{-1} with an intensity ratio (I_{2D}/I_G) of ≈1.17 (black line in Figure S2a, Supporting Information). A lack of a noticeable D-band (≈1330 cm^{-1}) indicates high-quality graphene without any significant defects or disorder within the sp^2-hybridized carbon arrangement. Then, the graphene was transferred onto the PET substrate, and the Raman spectra of bare PET and graphene on PET were collected (blue and red lines in Figure S2a, Supporting Information). In the range of 1000–3000 cm^{-1}, multiple Raman peaks from the PET film are more prominent than those of graphene, but the 2D-band of graphene at 2668 cm^{-1}, originating from two phonons near the **K** point, only appeared after the graphene transfer (Figure S2b, Supporting Information). This is consistent with previous studies[26] and confirms successful graphene transfer onto the PET film. We also constructed raster-scanned Raman intensity maps over the line-patterned graphene on the PET film. **Figure 2**a shows an optical microscope image of the bottom layer of the tactile sensor ($10 \times 10\ mm^2$), and the corresponding spatially resolved Raman intensity ratio (I_{2D}/I_G) is shown in Figure 2b. The intense region in the Raman intensity map is almost identical to the region where the graphene electrodes are patterned, indicating that the graphene is clearly defined and maintains its structural integrity without damage or degradation.

Figure 2c shows the tactile sensor exhibiting high transparency, which is capable of clearly showing backlit displays without any interference or decline in visibility. The transmittance of each component of the sensor was quantitatively investigated using an UV–vis spectrophotometer, as shown in Figure 2d. Considering the transmittance of the top and bottom PET layers (≈73.6%), the absorptions by graphene and stacked graphene are only 2.7% and 5.5% at a wavelength of 550 nm,

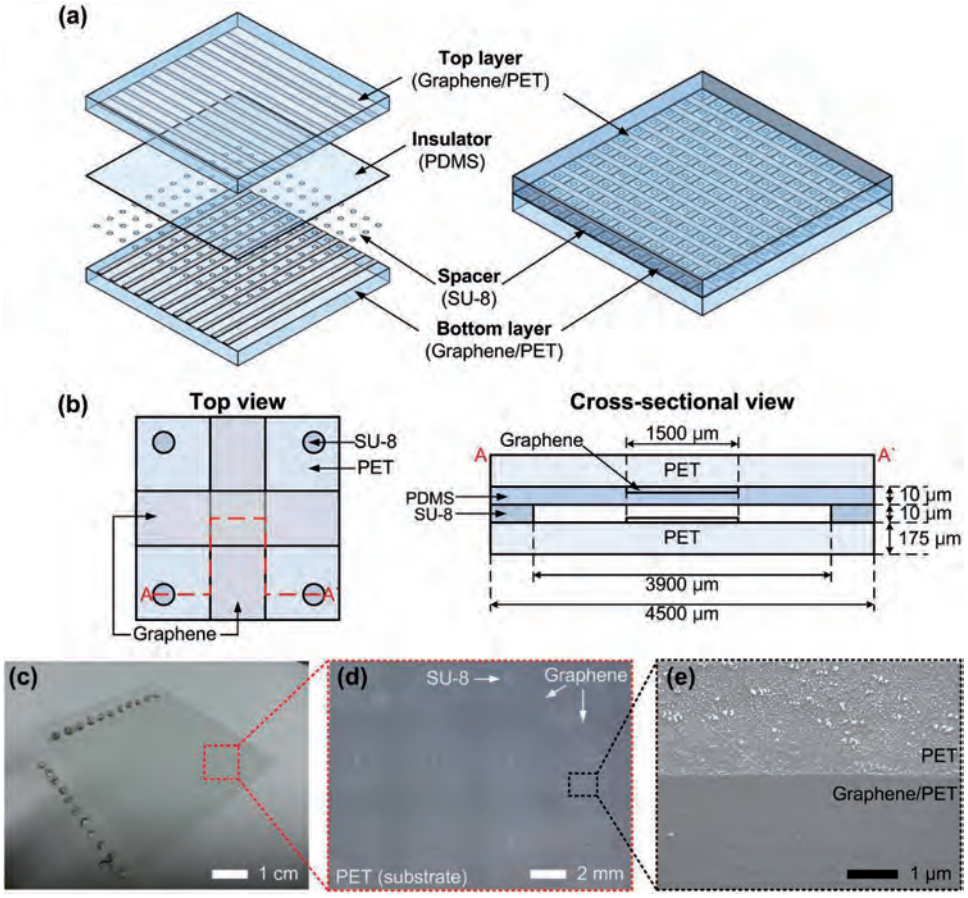

Figure 1. Flexible and transparent capacitive tactile sensor based on graphene electrodes. a) Schematic illustration of the sensor array composed of graphene-patterned top and bottom PET layers, PDMS insulator, and SU-8 spacers. b) Top and cross-sectional views of a single tactile cell with dimensions. The intersections of top and bottom graphene electrodes ($1500 \times 1500\ \mu m^2$) on PET films form a capacitor (calculated initial capacitance ≈1.38 pF) with a 20 μm gap between them. c) Photograph of as-fabricated tactile sensor consisting of a 10×10 tactile cell array. d) Enlarged optical microscope image of the sensor showing graphene electrodes and SU-8 spacers on PET substrate. e) SEM image of the boundary between patterned graphene and PET film.

respectively. The excellent transmittance of graphene, which originates from its atomic thickness, is not only superior to other transparent brittle electrode materials (such as indium tin oxide, ITO, and indium zinc oxide, IZO) but also shows less spectral variance across the visible spectrum. These optical properties make graphene suitable for use in touch screen applications, which requires the penetration of visible light through the tactile sensor. Moreover, the entire transparency of the sensor would be further improved when using thinner PET or more transparent substrates such as polycarbonate.

Figure 3 shows the pressure-sensing characteristics of our graphene-based tactile sensor. The measured initial capacitance (C_0) was 1.33 pF, which is close to the theoretical value of 1.38 pF estimated using the formula $C = 1/[(d_s/\varepsilon_0 A) + (d_i/\varepsilon_i \varepsilon_0 A)]$, where d_s and d_i are the thickness of the SU-8 spacer and PDMS insulator respectively, ε_0 and ε_i are the permittivity in the free space and the relative permittivity respectively of the PDMS, and A is the overlapping area between top and bottom graphene electrodes. To investigate changes to the capacitance of the sensor with respect to applied pressure, the pressure applied on the center of single cell was swept from 0 to 30 kPa and back to 0 kPa for 10 s at each step. The corresponding relative change in capacitance of the sensor ($\Delta C/C_0$) was continuously measured along with the pressure and plotted against time, as shown in Figure 3a. The capacitance increases (decreases) monotonously and simultaneously with the increase (decrease) in applied pressure. The capacitance continuously increases up to the pressures of 16 kPa, then flattens when the pressure exceeds 16 kPa. This is due to the contact between the top PET layer and PDMS insulator, and further increasing the pressure beyond this point squeezes the PDMS, which leads to slight changes in the capacitance. Given that the typical pulse or pressure generated by jugular vein, radial artery, finger touch, and motion are about 2, 4, 10, and 25 kPa, respectively.[5,7] The tested sensing range of 0–30 kPa would be suitable for monitoring human physiological signals and daily activities. We also evaluated the dependence of sensing characteristics on the position and area of applied pressure onto single tactile cell (Figures S3 and S4, Supporting Information). The $\Delta C/C_0$ was slightly deviated depending on the position and area, but nevertheless the tactile cell sensitively recognized the input pressures.

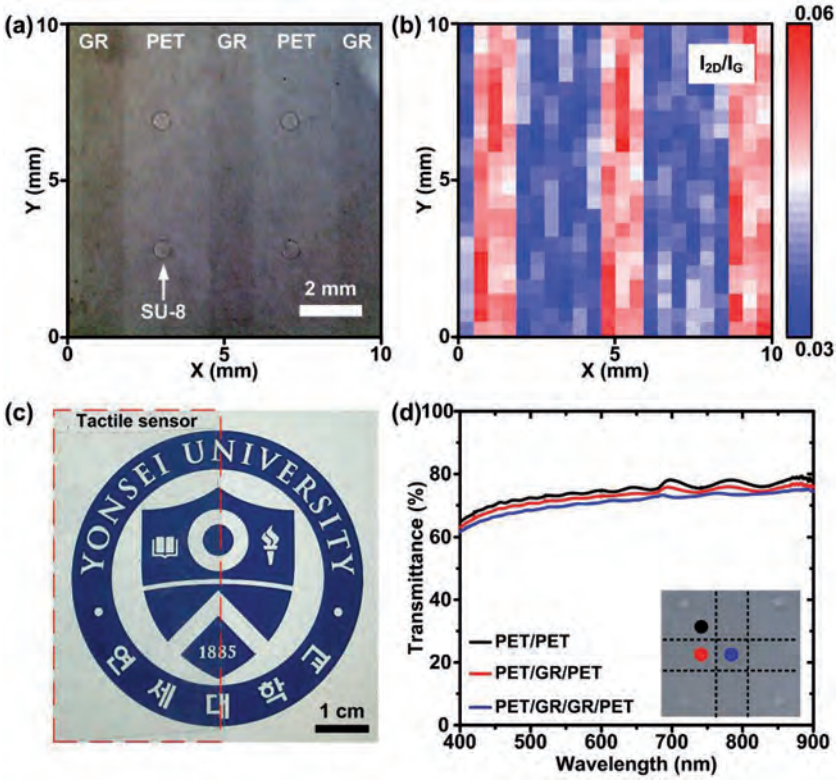

Figure 2. Optical characteristics of the tactile sensor. a) Optical microscope image of the bottom layer of the sensor (10×10 mm^2) and b) the corresponding Raman intensity map of 2D-band to G-band intensity ratio (I_{2D}/I_G). As the graphene exhibits a 2D-band at 2668 cm^{-1}, the Raman intensity map clearly identifies the patterned graphene electrodes. c) Photograph of the tactile sensor showing transparency, which is capable of displaying a backlit image without interference. d) Optical transmittance spectra of the PET/PET (black line), PET/graphene/PET (red line), and PET/graphene/graphene/PET (blue line) and the corresponding microscope image (inset). The optical absorption by graphene is only 2.7% at a wavelength of 550 nm.

The sensitivity of a capacitive tactile sensor (S) can be defined as $S = (\Delta C/C_0)/P$, where P is the applied pressure. The sensitivities of the sensor are calculated as 6.55 and 1.15% kPa^{-1} for the pressure ranges of 0–16 and 16–30 kPa, respectively. Owing to the air gap which enables effective deformation of the top layer under applied pressure, the sensitivity of our tactile sensor is higher than those in previous reports, which used a viscoelastic polymer as the dielectric layer.[12,14,19] To better elucidate the improvement of the sensitivity using air gap over polymer dielectrics, finite element analysis (FEA) of the deflection of the top layer against the applied pressure was conducted (see Experimental Section for a detailed simulation model). This result shows that the air gap facilitates more deflection of the top layer under applied pressure, inducing a larger increase in capacitance even compared to a dielectric layer that has very low elastic modulus (e.g., Ecoflex) (Figure S5, Supporting Information). Some of the previous tactile sensors that utilized microstructured or ionic gel dielectric layers reported higher sensitivity.[5,7,27] However, their flexibility or transparency was limited because they relied on intrinsically brittle or opaque electrodes (e.g., ITO or metal). Moreover, crosstalk-free recognition of external pressure between the adjacent cells still remained a significant challenge (see Table S1 in the Supporting Information for a detailed comparison between our sensor and other recently reported flexible capacitive tactile sensors). It is expected that the sensitivity and sensing range can be tailored by tuning the structural parameters, such as top layer stiffness, spacer and insulator thickness, electrode size, and in-plane distance between the spacers.[20] We also evaluated the hysteresis of the sensor by comparing the changes in capacitance with respect to the increase and decrease of pressure cycle. As shown in Figure 3b, no hysteresis is observed in the applied pressure range, which can be mainly attributed to the presence of the air gap instead of viscoelastic dielectric layer.

A transient response of the sensor was studied under pressure loading/unloading cycles for various pressures (Figure 3c) and frequencies (Figure S6, Supporting Information). The sensor operated stably and exhibited immediate response to the loaded/unloaded pressure. Response and relaxation time are important factors of tactile sensors that must be considered in order to minimize the response lag of the sensor. To quantify the response and relaxation times, the time-resolved response for one loading cycle (applied pressure of 8 kPa) was analyzed, and the sensor showed rapid response and relaxation times (≈70 ms) (Figure 3d). The response and relaxation times of our sensor are shorter than those of typical polymer-based tactile sensors which exhibit significant viscoelastic behavior.[12] In fact, the response and relaxation time are dependent on the performance of the pressure-loading apparatus, and the pressure input in our experiment cannot be a perfect step function. Thus, the response and relaxation times would be less than 70 ms when ideal step pressure is applied. To verify the durability and stability of the sensor, the changes in capacitance were measured by applying repeated pressure (8 kPa) for 2500 cycles (2 s for each cycle). The result, as shown in Figure 3d, reveals that the sensor retains a stable response upon repeated loading/unloading cycles without any noticeable degradation, demonstrating the excellent stability and durability of the sensor.

Next, we investigated a tactile sensor array that could yield spatial pressure information. For accurate multitouch recognition, each tactile cell should be able to sense pressure independently of adjacent cells, without crosstalk effects. We first performed FEA of the deflection of the top layer on a 3×3 sensor array to examine the crosstalk. **Figure 4**a shows the top-view schematic of the sensor array and the corresponding FEA result, which displays the distribution of top layer deflection under 8 kPa pressure applied on the center of the tactile cell with the area of 1.77 mm^2 (position O). The simulated center deflection of the center cell was ≈5.23 μm, while the adjacent cells (A, B, C, and D) showed no considerable deflection of the

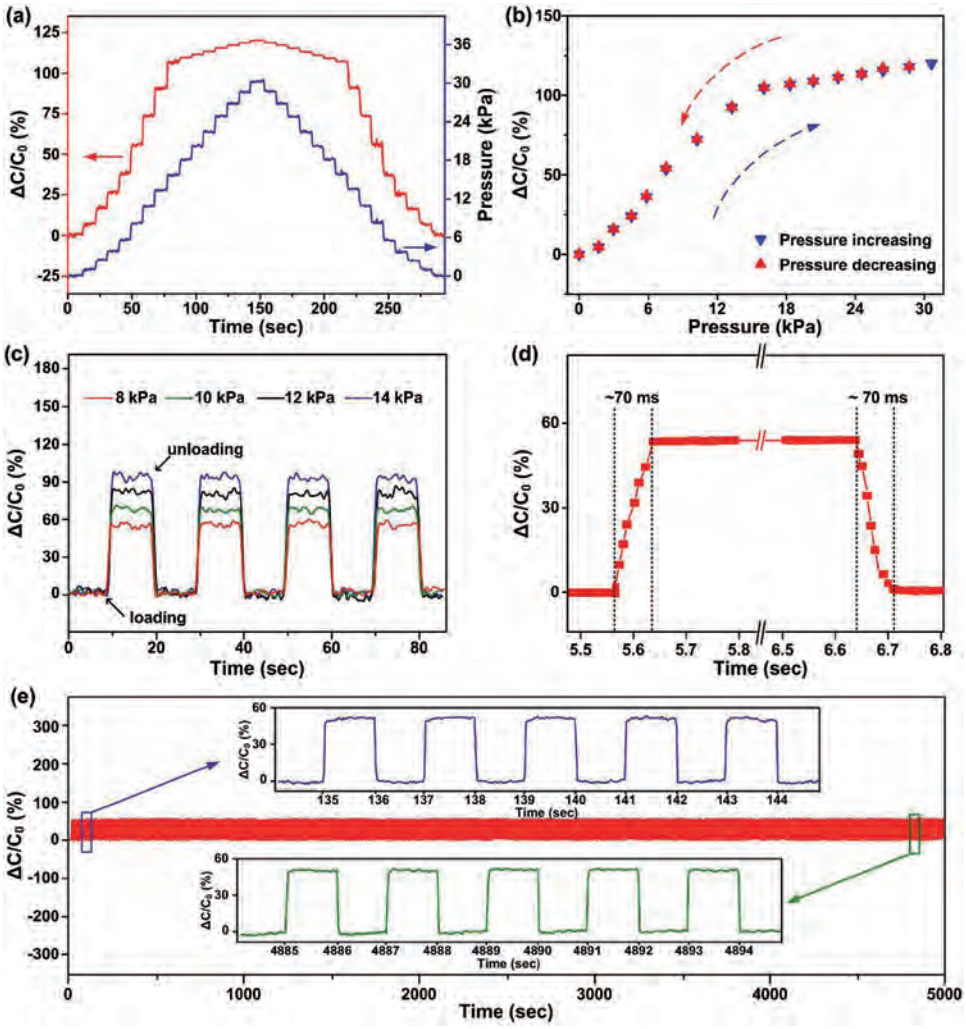

Figure 3. Pressure-sensing characteristics of capacitive tactile sensors based on graphene electrodes. a) Dynamic pressure loading (blue line) and the corresponding relative change in capacitance of the single tactile cell (red line). The capacitance was continuously measured, while the pressure was swept from 0 to 30 kPa and back to 0 kPa for 10 s duration per sequence. The capacitance immediately changes with respect to the change of applied pressure. b) Relative change of the capacitance as a function of applied pressure and hysteresis-free pressure sensing. The capacitance increases (decreases) monotonously when the applied pressure increases (decreases) without any hysteresis. The sensitivities of the sensor are 6.55 (0–16 kPa) and 1.15% kPa^{-1} (16–30 kPa). c) Transient responses of the sensor under repetitive loading/unloading cycles for various pressures (8, 10, 12, and 14 kPa). d) Time-resolved responses for one loading and unloading cycle (8 kPa), which shows response and relaxation times of 70 ms. e) Real-time changes in capacitance for 2500 loading/unloading cycles (2 s for each cycle) with an applied pressure of 8 kPa, indicating outstanding repeatability and stability of the sensor.

top layer. The linear center deflection against the applied pressure (0.65 μm kPa^{-1}) was much higher than in the adjacent cells (1.3×10^{-3} μm kPa^{-1}), as plotted in Figure 4b. Even though the pressure was applied over a broader area of 13.85 mm^2 in the center of the cell, the sensor exhibited no significant crosstalk as confirmed by FEA (Figure S7, Supporting Information).

The crosstalk of the sensor was then experimentally verified by measuring simultaneous changes in the capacitance of the cell-O and adjacent cells (A, B, C, and D) under loading at the center. The capacitance of the cell-O changes dramatically under 8 kPa loading cycles, but the other adjacent cells showed no detectable signals (Figure S8, Supporting Information). Figure 4c presents the changes in capacitance of five cells as a function of pressure applied on the cell-O; the capacitance of the cell-O shows high pressure sensitivity, while the adjacent cells remain insensitive to the applied pressure. Both the simulation and experimental results validate the negligible crosstalk effect of our sensor, unlike previously reported tactile sensor arrays where neighboring cells are not isolated.[12,20] In our sensor design, the SU-8 spacers efficiently eliminate crosstalk between each cell by suppressing pressure transmission through deformation of the top layer.

In order to verify crosstalk-free and multitouch recognition, we designed a pixelated 6 × 6 array and measured the changes in capacitance of each cell under multiple loads at different locations. Figure 4d shows the changes in capacitance of the 36 cells against two different pressures (6 and 12 kPa) and locations (C_{25}, C_{43} in the left panel and C_{33}, C_{43} in the right panel

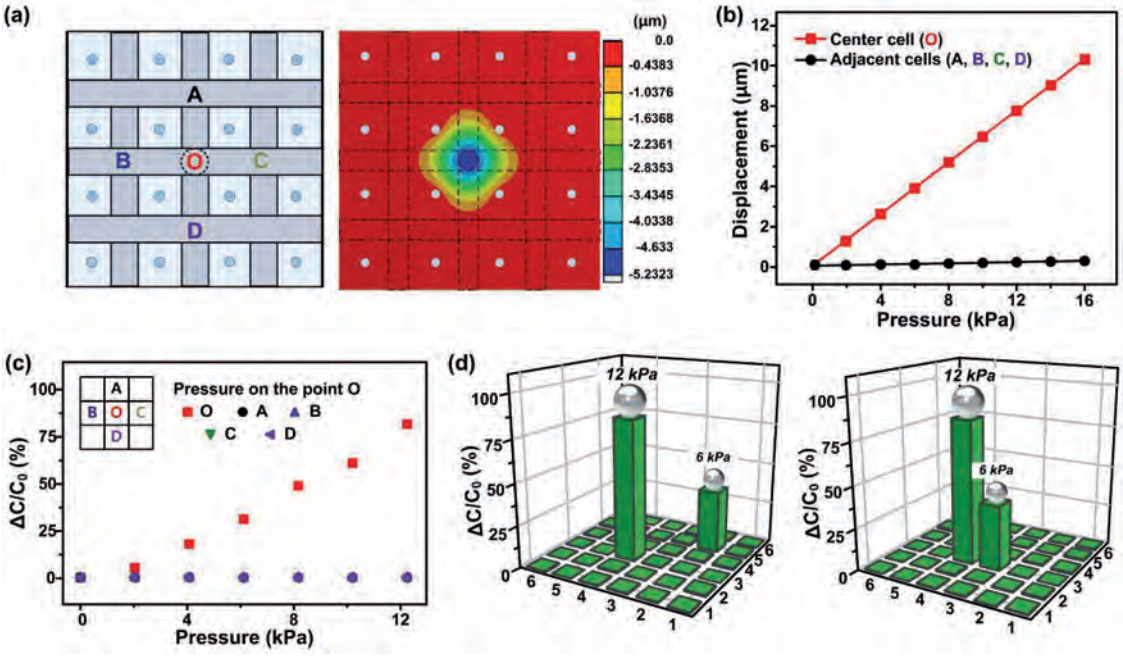

Figure 4. Crosstalk-free, multipoint recognition of flexible and transparent tactile sensors. a) Schematic illustration of the 3 × 3 tactile cell array and FEA result for deflection of the top layer under 8 kPa pressure applied on the center of cell-O (each cell area = 1.77 mm^2). b) The center deflection of the top layer of cell-O increases with increasing applied pressure up to 16 kPa, while the adjacent cells (A, B, C, and D) showed no significant deflection. c) Changes in capacitance of the five cells against different pressures applied on the cell-O. There is good agreement between the FEA and experimental results, indicating negligible crosstalk effect in the sensor. d) Crosstalk-free, multitouch recognition of the tactile sensor pixelated to a 6 × 6 array configuration.

in Figure 4d). When either pressure was applied on the C_{25} and C_{43} area, the capacitance of these cells increased by 33.84% and 76.52%, respectively. Similarly, the capacitance of the two adjacent cells (C_{33} and C_{43}) also changed 34.15% and 77.01%, respectively. The other cells, where pressure was not applied, showed no significant changes in capacitance. We also demonstrated that three different cells simultaneously recognized input pressures and exhibited similar sensing characteristics without crosstalk (Figure S9, Supporting Information). The results indicate that the sensor array can sensitively and independently recognize both magnitude and position of applied pressure in multiple locations.

An important improvement of tactile sensors, in order to widen their applicability, is sufficient mechanical flexibility to allow for stable operation under bending conditions. **Figure 5**a shows a photograph of the flexible tactile sensor array subjected to bending. The flexibility of the tactile sensor was examined by measuring capacitance changes of the center cell in the array under various bending radii (Figure 5b). The capacitance increases as the bending radius decreases and reaches ≈6.4%

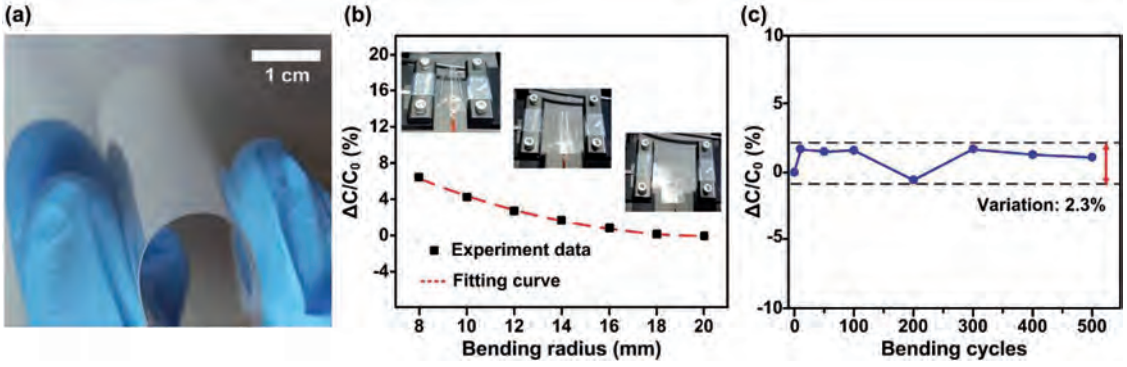

Figure 5. Mechanical flexibility of the tactile sensor. a) Photograph of the tactile sensor array displaying high flexibility. b) Relative change in capacitance of the center cell in the sensor array under various bending radii of 8–20 mm. The relative change in capacitance only deviates ≈6.4% at a bending radius of 8 mm (corresponding strain of 4.6%). c) Relative change in capacitance measured for 500 bending/relaxing cycles at a bending radius of 8 mm. The insignificant variation (2.3%) over 500 cycles denotes the high mechanical flexibility and electrical reliability of the sensor.

at a radius of 8 mm (strain of 4.6%). Nevertheless, the capacitive responses due to external bending are not significant as the change in signal resulting from pressure input. Notably, unlike brittle transparent electrodes such as ITO and IZO (which easily fracture under strains of ≈1%[28]), the capacitance recovered to its initial value with no permanent changes, demonstrating robust mechanical flexibility of the graphene electrode. To evaluate the durability of the sensor against bending, we conducted cyclic tests with repeated bending and relaxing. The variation of the capacitance change is <2.3% over 500 cycles of bending at a radius of 8 mm (Figure 5c), indicating excellent electrical and mechanical reliability of the sensor.

Finally, we studied the effect of temperature and humidity on the capacitive response, since these flexible tactile sensors are usually in contact with various surfaces which have different temperatures and can be exposed to transitional environments. The capacitance of the sensor exhibits negligible changes under variable temperature (23–60 °C, Figure S10, Supporting Information). This immunity to temperature changes is advantageous compared to resistive-type tactile sensors that are temperature-responsive,[6] providing an important advantage for diverse applications. The capacitance of the sensor was also measured under different humidity conditions. As the relative humidity (RH) increased from 30% to 97.1%, the capacitance increased slightly (Figure S11, Supporting Information). This increase is due to the fact that water molecules permeate through the air gap, resulting in increased relative permittivity in the sensor. This humidity effect can be minimal unless the tactile sensor is exposed to environments where humidity changes are rapid and intense. Although the sensor was operated under rapidly changing humidity, the change in capacitance against pressure loading would be still detectable as the humidity only changes the initial capacitance. Moreover, additional packaging would prevent the permeation of water molecules through the air gap and may provide the sensor with perfect immunity to humidity changes.

3. Conclusion

We have demonstrated a graphene-based capacitive tactile sensor that is flexible, fully transparent, and highly sensitive. The graphene electrode provides remarkable electrical reliability and mechanical flexibility with high optical transparency. The air gap between the graphene electrodes offers a high sensitivity of 6.55% kPa^{-1} and fast response/relaxation time of 70 ms without hysteresis. We also observed that the sensor exhibited high reliability against repeated bending over 500 cycles at a bending radius of 8 mm. The sensitivity and sensing range can be easily controlled by tuning the structural dimensions of the sensor. Notably, we have verified that structural isolation of each cell by the spacers prevents crosstalk between adjacent cells, as verified by FEA and other experiments. Accordingly, the pixelated sensor array successfully recognizes the spatial distribution of any applied pressure. Based on the outstanding performance, the scalability of graphene synthesis and transfer, and the compatibility with standard microfabrication, our graphene-based tactile sensor will provide meaningful opportunities for the development of portable/wearable devices, large-scale touch screens, and other similar structures.

4. Experimental Section

Fabrication of Tactile Sensor: Monolayer graphene synthesized on copper foil via chemical vapor deposition was transferred onto 175 µm thick PET substrates using a wet transfer process. To define the electrodes, 1.5 µm thick photoresist (GXR-601, AZ electronic materials) was patterned onto the graphene using photolithography. The exposed graphene was etched by O_2 plasma with 100 W for 7 s followed by complete removal of the photoresist with acetone. For spacer fabrication, 10 µm thick SU-8 was patterned on the PET film using photolithography. In parallel, 10 µm thick PDMS was spin-coated on the other graphene-transferred PET film to avoid short circuiting between the top and bottom graphene. Then, the PDMS was exposed to 70 W N_2 plasma for 120 s to form amino groups which can react and bond with epoxy groups on the SU-8 surface at high temperatures, using a plasma process system (COVANCE-MP, Femto Science). Finally, the top layer was aligned to the bottom layer using an optical microscope alignment system and bonded together at 120 °C for 1 h.

Characterization of Tactile Sensor: The morphology of the patterned graphene was investigated by field emission scanning electron microscopy (FE-SEM, JEOL-7800F). Raman spectra were obtained using a Horiba Jobin Yvon LabRam Aramis with 50 mW Ar-ion laser beam (λ = 532 nm) with a spot diameter of ≈1 µm. We used a UV–vis spectrophotometer (V650, JASCO) to obtain optical transmittance spectra. All capacitance measurements were carried out using an LCR meter (E4980A Precision LCR meter, Agilent) at 300 kHz with a 1 V AC signal at room temperature in air. The magnitude and frequency of the force were controlled by a universal measurement system (UMP 100, Teraleader). Force gauges (tip diameter: 2 and 2.53 mm) were used to apply force on a specific tactile cell. To verify the effect of temperature on the sensor, we measured the capacitance change in a forced convection oven over a temperature range of 23–60 °C. The capacitance of the sensor was measured at various RH conditions (30–97.1%) using a customized humidity control chamber.

Finite Element Analysis: 3D modeling and FEA were performed using 3D computer-aided design software (Solid Works 2011) and a finite element program (ANSYS 16.2), respectively. The Young's modulus values of PET, SU-8, PDMS, and Ecoflex was set to 3.5, 2, 2×10^{-3}, and 6×10^{-5} GPa respectively, with Poisson's ratios of 0.4, 0.22, 0.4999, and 0.49 for PET, SU-8, PDMS, and Ecoflex. The boundary condition for the bottom layer was fixed in all directions, and a unidirectional force perpendicular to the top surface was applied on top of the cell.

Supporting Information

Supporting Information is available from the Wiley Online Library or from the author.

Acknowledgements

This research was supported by Basic Science Research Program through the National Research Foundation of Korea (NRF) funded by the Ministry of Science, ICT and future Planning (NRF-2015R1A2A1A01005496) and by the Ministry of Education (NRF-2016R1D1A1B03932028).

Conflict of Interest

The authors declare no conflict of interest.

Keywords

crosstalk-free, flexibility, graphene, tactile sensors, transparency

Received: September 4, 2017
Published online:

[1] J. Yoon, W. Park, G. Y. Bae, Y. Kim, H. S. Jang, Y. Hyun, S. K. Lim, Y. H. Kahng, W. K. Hong, B. H. Lee, H. C. Ko, *Small* **2013**, *9*, 3295.
[2] S. Pyo, W. Kim, H. I. Jung, J. Choi, J. Kim, *Small* **2017**, *13*, 1700918.
[3] T. Chen, Y. Xue, A. K. Roy, L. Dai, *ACS Nano* **2014**, *8*, 1039.
[4] a) Y. Cheng, R. Wang, H. Zhai, J. Sun, *Nanoscale* **2017**, *9*, 3834; b) S. Kang, J. Lee, S. Lee, S. Kim, J. Kim, H. Algadi, S. Al-sayari, D. Kim, D. Kim, T. Lee, *Adv. Electron. Mater.* **2016**, *2*, 1600356.
[5] M. L. Jin, S. Park, Y. Lee, J. H. Lee, J. Chung, J. S. Kim, J. S. Kim, S. Y. Kim, E. Jee, D. W. Kim, J. W. Chung, S. G. Lee, D. Choi, H. T. Jung, D. H. Kim, *Adv. Mater.* **2017**, *29*, 1605973.
[6] M. Park, Y. J. Park, X. Chen, Y. K. Park, M. S. Kim, J. H. Ahn, *Adv. Mater.* **2016**, *28*, 2556.
[7] S. H. Cho, S. W. Lee, S. Yu, H. Kim, S. Chang, D. Kang, I. Hwang, H. S. Kang, B. Jeong, E. H. Kim, S. M. Cho, K. L. Kim, H. Lee, W. Shim, C. Park, *ACS Appl. Mater. Interfaces* **2017**, *9*, 10128.
[8] X. Wang, L. Dong, H. Zhang, R. Yu, C. Pan, Z. L. Wang, *Adv. Sci.* **2015**, *2*, 1500169.
[9] S. Gong, W. Schwalb, Y. Wang, Y. Chen, Y. Tang, J. Si, B. Shirinzadeh, W. Cheng, *Nat. Commun.* **2014**, *5*, 3132.
[10] D. Lee, H. Lee, Y. Jeong, Y. Ahn, G. Nam, Y. Lee, *Adv. Mater.* **2016**, *28*, 9364.
[11] X. Wang, Y. Gu, Z. Xiong, Z. Cui, T. Zhang, *Adv. Mater.* **2014**, *26*, 1336.
[12] D. J. Lipomi, M. Vosguertichain, B. C. Tee, S. L. Hellstrom, J. A. Lee, C. H. Fox, Z. Bao, *Nat. Nanotechnol.* **2011**, *6*, 788.
[13] S. Y. Kim, S. Park, H. W. Park, D. H. Park, Y. Jeong, D. H. Kim, *Adv. Mater.* **2015**, *27*, 4178.
[14] S. J. Woo, J. H. Kong, D. G. Kim, J. M. Kim, *J. Mater. Chem. C* **2014**, *2*, 4415.
[15] V. Maheshwari, R. Saraf, *Angew. Chem., Int. Ed.* **2008**, *47*, 7808.
[16] M. L. Hammock, A. Chortos, B. C. K. Tee, B. H. Tok, Z. Bao, *Adv. Mater.* **2013**, *25*, 5997.
[17] J. Wang, J. Jiu, M. Nogi, T. Sugahara, S. Nagao, H. Koga, P. He, K. Suganuma, *Nanoscale* **2015**, *7*, 2926.
[18] J. Lee, H. Kwon, J. Seo, S. Shin, J. H. Koo, C. Pang, S. Son, J. H. Kim, Y. H. Jang, D. E. Kim, T. Lee, *Adv. Mater.* **2015**, *27*, 2433.
[19] W. Hu, X. Niu, R. Zhao, Q. Pei, *Appl. Phys. Lett.* **2013**, *102*, 083303.
[20] B. C. Tee, A. Chortos, R. R. Dunn, G. Schwartz, E. Eason, Z. Bao, *Adv. Funct. Mater.* **2014**, *24*, 5427.
[21] T. Li, H. Luo, L. Qin, X. Wang, Z. Xiong, H. Ding, Y. Gu, Z. Liu, T. Zhang, *Small* **2016**, *12*, 5042.
[22] W. J. Yu, S. Y. Lee, S. H. Chae, D. Perello, G. H. Han, M. Yun, Y. H. Lee, *Nano Lett.* **2011**, *11*, 1344.
[23] B. Zhu, Z. Niu, H. Wang, W. R. Leow, H. Wang, Y. Li, L. Zheng, J. Wei, F. Huo, X. Chen, *Small* **2014**, *10*, 3625.
[24] T. Yang, W. Wang, H. Zhang, X. Li, J. Shi, Y. He, Q. H. Zheng, Z. Li, H. Zhu, *ACS Nano* **2015**, *9*, 10867.
[25] S. Chun, Y. Kim, H. Jung, W. Park, *Appl. Phys. Lett.* **2014**, *105*, 041907.
[26] Z. Li, I. A. Kinloch, R. J. Young, K. S. Novoselov, G. Anagnostopoulos, J. Parthenios, C. Galiotis, K. Papagelis, C. Y. Lu, L. Britnell, *ACS Nano* **2015**, *9*, 3917.
[27] B. Nie, R. Li, J. Cao, J. D. Brandt, T. Pan, *Adv. Mater.* **2015**, *27*, 6055.
[28] D. M. Sun, C. Liu, W. C. Ren, H. M. Cheng, *Small* **2013**, *9*, 1188.

